NANOSYSTEMS: PHYSICS, CHEMISTRY, MATHEMATICS, 2014, 5 (4), P. 579–589

A FACILE ROUTE OF COUPLING OF ZnO NANORODS BY CdS NANOPARTICLES USING CHEMICAL BATH DEPOSITION

N. S. Kozhevnikova, O. I. Gyrdasova, A. S. Vorokh, I. V. Baklanova, L. Yu. Buldakova

Institute of Solid State of the Ural Branch of Russian Academy of Sciences, Ekaterinburg, Russia

kozhevnikova@ihim.uran.ru

PACS 71.20.Nr, 71.55.Gs, 78.30.Fs

Cadmium sulfide nanoparticles (NPs) coupled to zinc oxide nanorods (NRs) were synthesized in a two step deposition process at relatively low temperatures. The ZnO NRs were grown using solvothermal method, followed by the deposition of CdS NPs at 50 °C using *in-situ* and *ex-situ* synthesis from aqueous solutions. The samples were characterized by X-ray diffraction, scanning electron microscopy, and optical absorption. When the ZnO NRs are coated by the CdS NPs, the optical absorption is enhanced and band edge is shifted towards visible region as compared with ZnO NRs. Photocatalytic activity of the synthesized ZnO NRs / CdS NPs composites in the photooxidation of hydroquinone $C_6H_4(OH)_2$ in aqueous solution is closely connected with the coupling route.

Keywords: Cadmium sulfide nanoparticles, zinc oxide nanorods, coupled inorganic semiconductors, chemical bath deposition.

Received: 16 June 2014
Revised: 30 June 2014

1. Introduction

Inorganic nanostructures have become ideal systems for revealing novel phenomena at nanoscale, leading to a wide range of applications [1–3]. Depending upon the dimensionality and the capability of tailoring the morphology, they are becoming essential for smart and functional materials. Foremost, numerous research efforts have been concentrated on the environmental use of semiconductor inorganic materials as photocatalysts in processes such as the decomposition of toxic organic compounds and hydrogen production via water photolysis [4]. A variety of geometrical morphologies [5–8] are being investigated for the different semiconductor nanostructures to explore novel properties out of those materials. Among the various photocatalytic semiconductor materials, metal-oxide semiconductors such as ZnO (3.2 eV), TiO_2 (3.2 eV), α-Fe_2O_3 (3.1 eV) and WO_3 (2.8 eV) have been researched intensively as practically applicable photocatalysts, because of their high photocatalytic activities and economical synthetic routes [9, 10]. However, these single metal-oxide photocatalysts have wide band-gap energies, which are disadvantageous for the absorption and use of the visible light region of solar energy. To improve photocatalytic activities, composite semiconductor photocatalyst systems with different geometry [11–16] have received a great deal of attention because of two important reasons. First, in the composite semiconductor systems with different energy levels, wide band-gap semiconductors can utilize visible light by coupling narrow/mid band-gap semiconductors (CdS, In_2S_3, Bi_2O_3) which are visible light active materials [17, 18]. Second, charge injection from one semiconductor into another can lead to efficient and longer charge separation by reducing the electron – hole pair recombinations [19, 20]. The coupled semiconductors, in

particular, are attracting attention not only for their successful implementation in the photocatalytic degradation of organic pollutants, but also in renewable energy conversion [21, 22] as a new generation of solar cells.

Among the different photoactive semiconductor nanostructures, the ZnO based nanocomposites [12–14] gained extreme importance for its different advantages, such as direct band gap, ease of crystallization, anisotropic growth, nontoxicity, higher excitation binding energy of 60 meV, higher electron mobility (200 $cm^2V^{-1}s^{-1}$) and simplicity in tailoring the morphology. CdS (bulk band gap 2.42 eV) is one of the most appropriate sensitizer for ZnO. Recently, many groups have attempted to develop different synthetic routes for the efficient creation of CdS–ZnO heterojunctions with different morphology. The study of CdS/ZnO system for photocatalytic effect not only varies in synthesis technique but also has wide variety of efficiency, according to the structure of the composite. Different CdS–ZnO systems, e.g. flower-like CdS-ZnO nanocomposite [11], urchin like CdS@ZnO [16], nanotubes arrays of CdS/ZnO [23], partially or fully covered CdS nanoparticles on ZnO nanorods [24], ZnO/CdS core shell nanorods [14], CdS nanoparticles/ZnO nanowires heterostructure [25, 26] have been reported. Nevertheless, such key factors like the development of facile methods for the synthesis, surface modification, linking and sensitizing CdS NPs to ZnO still remain unsolved. This problem is very urgent, because despite the advantages known for using coupled semiconductors, the conversion efficiency of such structures is still not very high and requires further development. Two possible reasons for the low photovoltaic performance are the difficulty of assembling NPs into mesoporous oxide film and the presence of a large number of unpassivated or partially passivated surface states. These surface states can act as trap centers for holes and electrons, leading to lower photovoltage and photocurrent [27].

Today for the sensitization of semiconductor NPs to TiO_2, generally two routes are followed:

(i) *In-situ* synthesis and deposition of NPs by chemical bath deposition (CBD) [28] or successive ionic layer adsorption and reaction (SILAR) [29] method. In this route the NPs are directly grown onto the oxide material surface by the chemical reaction of respective ionic species.

(ii) *Ex-situ* route linking the synthesized colloidal NPs to the oxide material surface via a bifunctional linker [30].

Both routes have their own advantages and disadvantages. The former route shows better performance due to less spatial distance between the NPs and the substrate surface. While the latter route has an advantage of controlling the NPs properties like size and shape. In both routes, the growth rate is controllable by solution, pH, temperature and relative concentrations of the reactants in the bath solution.

In this work, we report our observations following the use of both routes for the coupling of CdS NPs to the ZnO nanorods (NRs) which were grown using the solvothermal method. We have analyzed the effect of chemical route on the coverage quality of ZnO NRs by CdS NPs. The structural and optical properties of the coupled semiconductor ZnO NRs – CdS NPs have been investigated. This composite semiconductor showed the visible light absorption and photocatalytic activity.

2. Experimental

2.1. Materials used

To synthesize ZnO NRs, the following precursors were used: zinc oxide ZnO, formic acid HCOOH and ethylene glycol $HO(CH_2)_2OH$. The precursors employed to synthesize CdS

NPs by CBD include cadmium chloride hydrate $CdCl_2{\cdot}2H_2O$, thiourea $SC(NH_2)_2$, aqueous ammonia (NH_4OH) (19 %) and ethylenediaminetetraacetic acid disodium salt dihydrate $C_{10}H_{14}N_2Na_2O_8$ (Na_2EDTA). Sodium hydroxide NaOH was used for adjusting the pH. Sodium sulfide nonahydrate $Na_2S{\cdot}9H_2O$ was used for synthesis of colloid CdS NPs. All the chemicals were purchased and used as procured for all stock solution preparations.

2.2. Preparation of ZnO NRs

Firstly, ZnO NRs were synthesized by solvothermal method based on the thermolysis of the organometallic complexes and reported elsewhere [31–33]. For the present investigation, the formate glycolate zinc complexes $Zn(HCOO)(OCH_2CH_2O)_{1/2}$ with fiber shaped crystals were pre-synthesized via two steps

$$ZnO + 2HCOOH + H_2O \Rightarrow Zn(HCOO)_2 \cdot 2H_2O, \tag{1}$$

$$\begin{gathered} Zn(HCOO)_2 \cdot 2H_2O + 1/2HOCH_2CH_2OH \Rightarrow \\ Zn(HCOO)(OCH_2CH_2O)_{1/2} + HCOOH \uparrow + 2H_2O. \end{gathered} \tag{2}$$

The latter interaction of zinc formate $Zn(HCOO)_2{\cdot}2H_2O$ with ethylene glycol was carried out at temperature not higher than 120 °C. The solid reaction products were separated from the liquid phase by vacuum filtration, washed with anhydrous acetone, and dried at 40 °C to remove acetone. Thermal decomposition of fibrous $Zn(HCOO)(OCH_2CH_2O)_{1/2}$ to ZnO in air is an exothermic process that occurred at 450 °C over 4 h. The post-annealed particles of the formed ZnO NRs acquired the fibrous shape of the $Zn(HCOO)(OCH_2CH_2O)_{1/2}$ precursor crystals.

2.3. Preparation of CdS aqueous colloid solution

To prepare stable aqueous colloidal solutions of CdS nanoparticles, solutions of 12.5 mM $CdCl_2$, 12.5 mM Na_2S, 12.5 mM Na_2EDTA were mixed at room temperature under continuous stirring. The starting concentration ratio of the precursor ions in a solution was equal to $Cd^{2+} : S^{2-} : EDTA^{4-} = 1 : 1 : 1$ [34,35]. While mixing the precursor solutions, two reactions occur:

$$CdCl_2 + Na_2EDTA \Rightarrow Cd(EDTA) + 2NaCl, \tag{3}$$

$$Cd(EDTA) + Na_2S \Rightarrow CdSv + Na_2EDTA. \tag{4}$$

Both aggregate and sedimentation stability of the colloidal solution is achieved through the formation of double ion and the adsorption-solvate layers at the adsorption of ions $EDTA^{4-}$ on the surface of the CdS disperse phase [34,35].

2.4. Coupling of ZnO NRs by CdS NPs

In-situ synthesis (CBD): The CdS NPs were deposited on ZnO NRs from a chemical bath containing: (i) 5 mM $CdCl_2$, 25 mM thiourea and 2 % NH_4OH at pH = 12.5 (sample 1); (ii) 5 mM $CdCl_2$, 25 mM thiourea and 10 mM Na_2EDTA at pH = 13.5 (adjusted with NaOH) (sample 2). In both cases, the ZnO NRs powder was immersed in the chemical bath solution for 180 min at 50 °C. Aqueous ammonia and Na_2EDTA solution act as a complexing agents forming intermediate cadmium complexes $[Cd(NH_3)_4^{2+}]Cl_2$ or [Cd(EDTA)] releasing cadmium ions. The alkaline medium provides sulfide ions via the conversion of thiourea to cyanamide.

During CBD the CdS NPs are directly grown onto the ZnO NRs surface by the overall chemical reactions of respective ionic species:

$$Cd(NH_3)_4Cl^{2+} + SC(NH_2)_2 + 2NH_4OH \Rightarrow CdS + H_2NCN + 4NH_3 + 2NH_4Cl + 2H_2O, \quad (5)$$

$$Cd(EDTA) + SC(NH_2)_2 + 2NaOH \Rightarrow CdS + H_2NCN + Na_2EDTA + 2H_2O. \quad (6)$$

Using ammonia complexes, $Cd(NH_3)_4Cl_2$ leads to supersaturation with respect to $Cd(OH)_2$ and as a result, to $Cd(OH)_2$ crystal formation at the first stage of the CBD process [36, 37]. The second stage leads to the CdS solid phase formation. The overall reaction (5) should be written as

$$Cd(NH_3)_4Cl_2 + 2NH_4OH \Rightarrow Cd(OH)_2 + 4NH_3 + 2NH_4Cl, \quad (7)$$

$$Cd(OH)_2 + SC(NH_2)_2 \Rightarrow CdS + H_2NCN + 2H_2O. \quad (8)$$

The presence of the Cd(EDTA) complex prevents formation of the oxygen containing compound while CdS synthesis and is described by (6).

Formation of $Cd(OH)_2$ phase is important synthetic factor for two reasons. Firstly, it is well known that interdiffusion occurs between the CdS sensitized layers during the annealing in oxide and chalcogenide solar cells [38]. Sulfur diffusion is responsible for the thinning of the CdS film and this may result in poor device performance. Oxygen has been shown to reduce the diffusion of S. The reason is likely the Cd–O bonds at the grain boundaries, which reduce the S diffusion [39]. Secondly, it is an experimental fact that high quality adherent CdS layers and films can be obtained from alkaline baths, which are in a formal sense supersaturated with respect to the precipitation of the oxygen containing compound, namely $Cd(OH)_2$, and this holds irrespective of the substrate employed and substance sensitized [40]. It is well known that the carboxylic group in the dyes plays vital role for the adsorption of the dyes upon oxide surface in quantum dot sensitized solar cells [41].

For these reasons we decide to synthesize ZnO–CdS composites both with and without $Cd(OH)_2$ and trace the influence of $Cd(OH)_2$ on microstructure and properties of composites.

Ex-situ synthesis (colloid synthesis): The powder of ZnO NRs was immersed into the aqueous colloid solution of CdS NPs and maintained for 180 min at 50 °C. The CdS NPs are then linked onto the ZnO NRs surface via the absorption processes (sample 3).

After the CBD and colloid synthesis, the powder samples were filtered, washed with deionized water and air dried.

2.5. Crystal structure, microstructure, optics and photocatalytic activity measurements

X-ray diffraction (XRD) patterns of ZnO NRs / CdS NPs composites were obtained using a Shimadzu MAXima-X XRD-7000 automatic diffractometer with CuKα ($\lambda = 1.5406$ Å) with 2θ angle step 0.03 ° and exposition time of 10 sec. The scanning electron microscopy (SEM) was carried out in order to analyze the microstructure and morphology of all synthesized samples using JEOL-JSM LA 6390. To confirm the change in bandgap, the UV and Vis spectra in the wavelength range of 300–700 nm ($BaSO_4$ was used as the standard) of bare ZnO NRs and ZnO NRs / CdS NPs composites were recorded using Shimadzu UV-2401 PC spectrophotometer.

To examine the photocatalytic activity, hydroquinone $C_6H_4(OH)_2$ (HQ) dye was chosen for the photodecomposition study. The ZnO NRs coupled by CdS NPs composite samples were immersed in 0.4 mM of HQ aqueous solution and irradiated by a blue light fluorescent lamp

with the emission maximum in the wavelength range of 440–460 nm. The remaining amounts of HQ in the solution were determined by voltammetry on a PU-1 polarograph at a potential sweep rate of 0.030 V/s.

3. Results and discussion

X-ray diffraction patterns of CdS–ZnO composites (Fig. 1) show narrow peaks of highly crystalline ZnO (space group No. 186, $P6_{3mc}$) and broad peaks of nanostructured CdS. The crystal structure of CdS can be identified as random close-packed structure (RCP) with an average lattice having unit cell parameters $a = 0.236$ nm and $c = 0.334$ nm [42]. The Cd and S atoms in the unit cell of the average lattice occupy single positions as $P6$ and 1(a) with the coordinates (0 0 z), where $z = 0$ and $1/\sqrt{24}$, respectively; the filling factor of these positions is 1/3. In sample 2, some broad peaks pointed to the high probability of ordering CdS nanoparticles to hexagonal closepacked structure (HCP, space group No. 186, $P6_{3mc}$). In sample 3, the crystal structure of CdS NPs is amorphous. Sample 1 contains crystalline $Cd(OH)_2$ (space group No. 164, $P - 3m1$) and phase ratio are equal ZnO : CdS : $Cd(OH)_2$ = 17 : 52 : 31. Samples 2 and 3 do not contained hydroxide, and CdS portion is 19 % (vol.) in sample 2, and less the 1 % in sample 3.

The photo gallery of Fig. 2 shows the typical SEM images of the synthesized ZnO and ZnO–CdS nanocomposite structure. Particles of bare ZnO are extended micrometer-sized aggregates with a fine fibrous structure (Fig. 2a) which may be called NRs. Fig. 2 (b–d) shows the morphology of ZnO NRs while coupling by CdS. To corroborate the chemical and phase analysis, EDX was carried out and the results show the existence of Cd, S, Zn and O elements in CdS–ZnO nanocomposites, but the atom space distribution in the samples 1–3 is quite different. On the scale of SEM, sample 1 is a mixture of ZnO NRs and well-shaped hexagonal prisms of nearly the same size in the micrometer range (Fig. 2b). With a focused beam, EDX exclusively confirmed Cd, O and S species were found inside these hexagonal prisms, therefore they are identified as $Cd(OH)_2$ polycrystals containing about 10 at.% of CdS. The highest concentration of CdS in sample 1 is located on the ZnO NRs surface. Sample 2 is also predominantly a mixture of ZnO NRs and nanocrystalline CdS particles (Fig. 2c). It is evident from Fig. 2d that the sample 3 is ZnO NRs – CdS NPs composite material formed by polycrystals of a nearly uniform fiber like morphology.

Image 2(a–d) clearly exhibits the porous nature of the ZnO NRs. This porous structure of ZnO helps in the coupling of CdS NPs, because when NPs are embedded on ZnO, NPs actually occupy these pores where they get adsorbed.

The fulfilled XRD phase analysis of sample 1 confirmed by SEM proves the reaction mechanism of CdS formation to be considered the same as proposed by Kitaev et al. [36] (see eq. 7, 8).

Figure 3 shows the optical absorption spectra of the of bare ZnO NRs and ZnO NRs / CdS NPs composite samples 1–3, which were synthesized according to the procedure described above. The increase in the absorption spectra of samples 1–3 at 420–480 nm suggests the presence of at least two phases, confirming XRD and SEM data. As can be seen from this figure, the fundamental absorption band edge of the ZnO NRs / CdS NPs composite is shifted toward lower energies with respect to the absorption band of the initial bare ZnO. In order to determine the effective band gaps, the absorption spectra were converted to the form $(\alpha h\nu)^2 = f(h\nu)$. The dependence of the absorption coefficient for ZnO as a direct band gap semiconductor on the frequency near the absorption edge is described by equation (9)

$$\alpha(\nu) = \left[A(h\nu - E_g)^{1/2}\right]/h\nu, \tag{9}$$

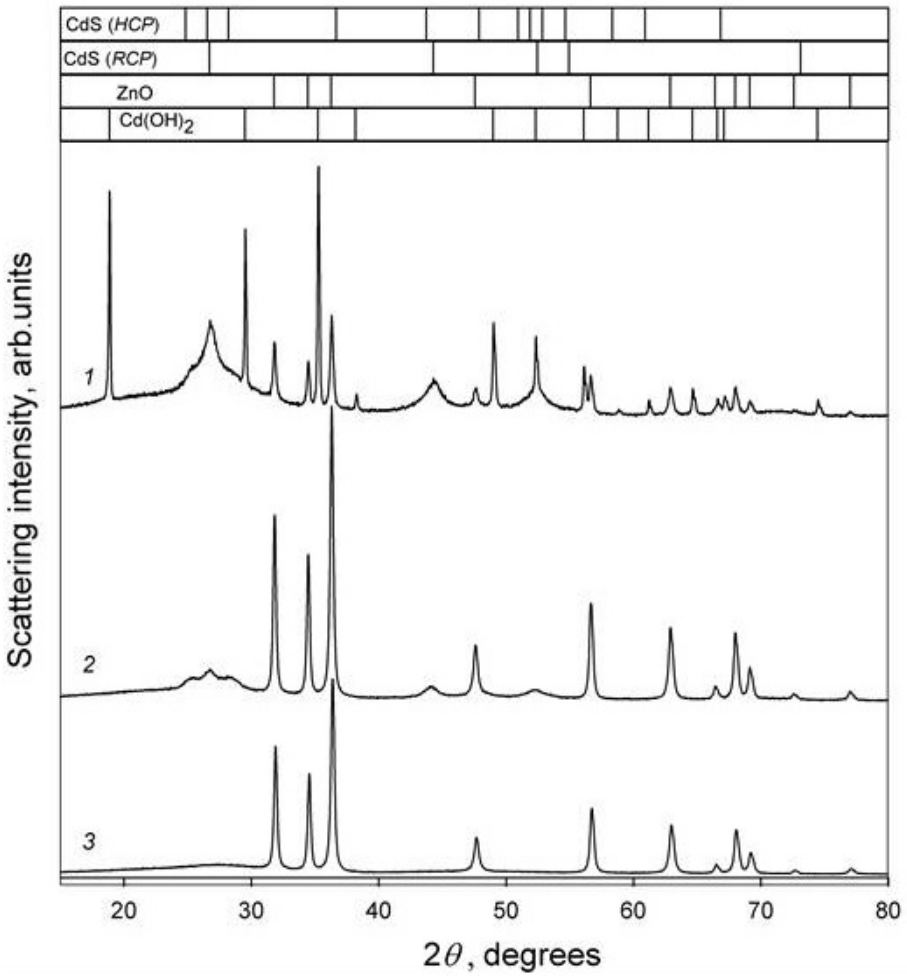

FIG. 1. X-ray diffraction patterns of ZnO-CdS nanocomposites. ZnO NRs are coupled by CdS NPs in aqueous solutions via following routes: 1 — *in-situ* CBD synthesis using ammonia complexes $Cd(NH_3)_4^{2+}$; 2 — *in-situ* CBD synthesis using EDTA complexes $Cd(EDTA)^{2-}$; 3 — *ex-situ* synthesis using pre-synthesized CdS colloid solution

where α is the absorption coefficient, $h\nu$ is the photon energy, E_g is the optical band gap, and A is a constant that does not depend on the frequency ν [43]. According to this equation, the optical band gap can be obtained by the extrapolation of the linear part of the $(\alpha h\nu)^2 = f(h\nu)$ to the intersection with the abscissa axis. The determined Eg values are presented in Table 1.

Optical absorption data suggest the following conclusions. The intensity of absorption from 440–480 nm after coupling ZnO NRs to CdS NPs increases with increased CdS content and reaches its maximum for sample 1. Furthermore, the blue shift of the absorption edge is due to exciton confinement in CdS NPs. For this reason, CdS NPs with size of 2 nm (sample 3) reduce the absorption intensity greatly from 440–480 nm.

To demonstrate the effects of visible light absorption ability of the ZnO NRs / CdS NPs composites on photocatalytic activity, we tested the samples under conditions similar to that of natural solar-light irradiation. The photocatalytic properties of the synthesized ZnO NRs / CdS NPs composites are examined using model reaction of HQ oxidation in aqueous medium. The kinetic curves of HQ oxidation, demonstrating a change in the HQ concentration with time under visible light irradiation (440-460 nm), are shown in Fig. 4. The inset of Fig. 4 shows

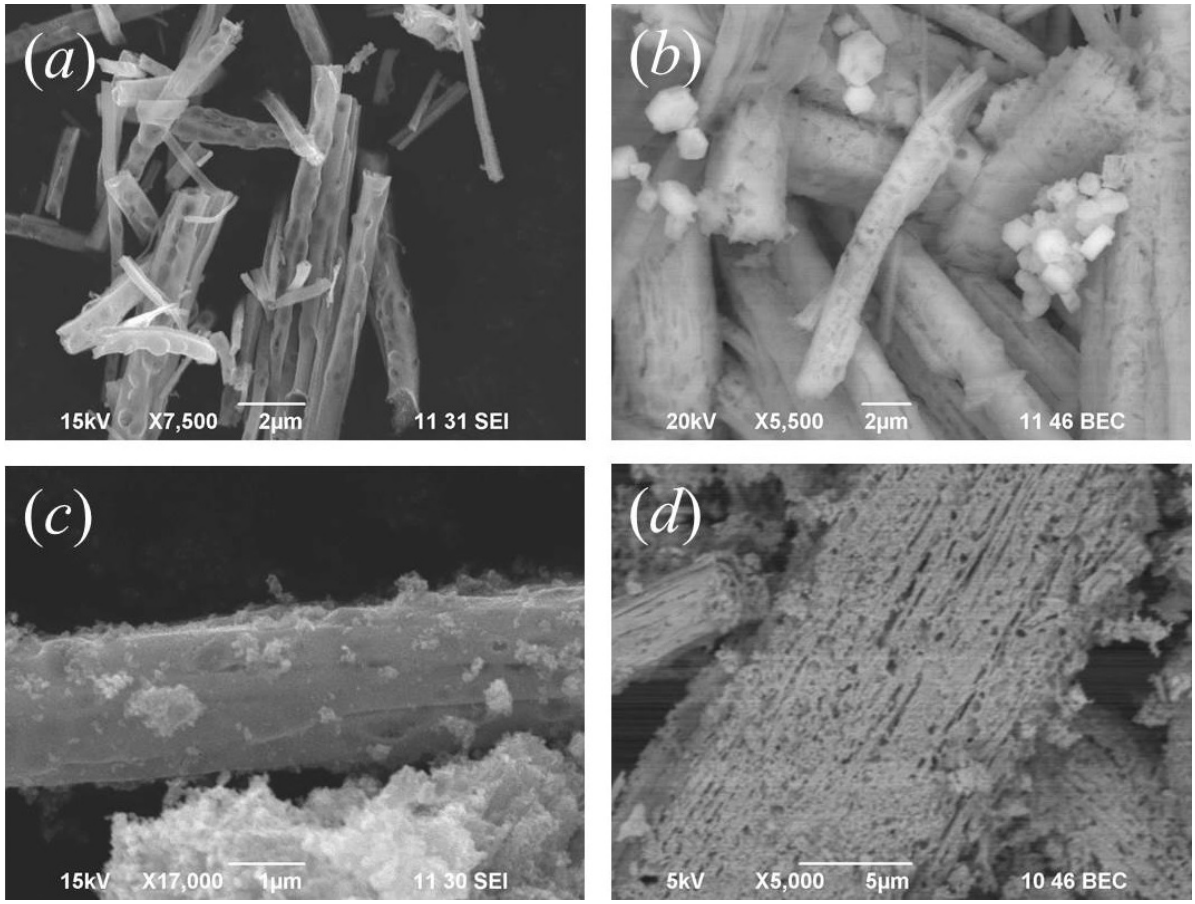

FIG. 2. Typical SEM images of bare ZnO NRs (a) and ZnO NRs / CdS NPs composite material (b–d). ZnO NRs are coupled by CdS NPs in aqueous solutions via *in-situ* CBD synthesis (b — sample 1, c — sample 2) and *ex-situ* synthesis in the pre-synthesized CdS colloid solution (d — sample 3)

the conversion degree of HQ to quinone after 8 hours of irradiation. The conversion degree represents the ratio of residual HQ concentration to the initial one. It is seen that the HQ oxidation rate increases in the series of reactions: solution without and in presence of ZnO NRs / CdS NPs composites. The highest rate and conversion degree of oxidation reaction is observed for sample 1.

Comparing the results for samples 1–3 obtained from XRD, optical and photocatalytic data, we suggest that the higher photocatalytic activity of the sample 1 in comparison with samples 2 and 3 (Fig. 4) is due to the higher content of CdS NPs in semiconductor composite (Table 1) and not to smaller particle size.

4. Conclusion

Semiconductor composite materials, consisting of CdS NPs embedded in a ZnO NRs, have been successfully produced by two step deposition process at relatively low temperatures. The ZnO NRs grown by solvothermal process were coupled by CdS NPs at 50 °C using *in-situ* and *ex-situ* routes in aqueous solutions. *In-situ* deposition of CdS NPs was carried out by CBD from solutions both supersaturated and unsaturated with respect to $Cd(OH)_2$ crystal phase. *Ex-situ* coupling ZnO NRs was held in pre-synthesized colloid solution of CdS NPs. Optical absorbance measurements show a blue shift of the Eg of CdS NPs due to the quantum

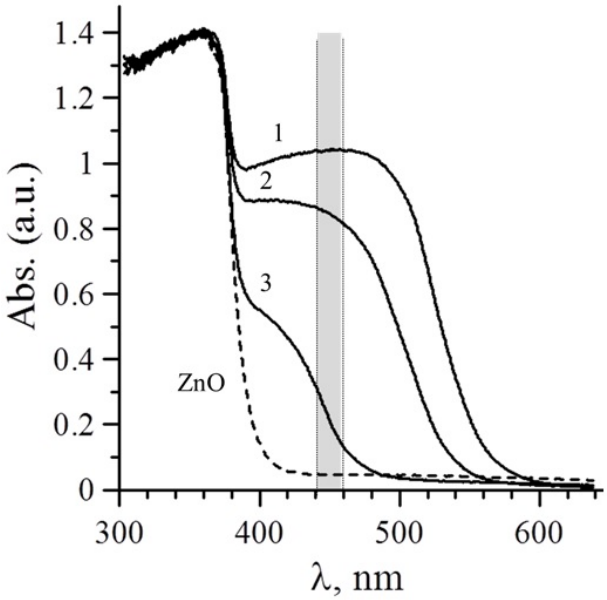

FIG. 3. Optical absorption spectra of uncoupled ZnO (experimental E_g = 3.23 eV) and ZnO NRs / CdS NPs composites (samples 1–3) obtained in UV and visible regions at room temperature. Visible light irradiation range while photocatalyzing HQ oxidation is highlighted by a gray bar

TABLE 1. Structural and optical characterization of CdS NPs in ZnO NRs / CdS NPs composites in dependence of coupling route. Experimental values of HQ conversion degree after oxidation in air in the presence of ZnO NRs / CdS NPs composites under irradiation at 440–460 nm for 12 h

Sample	Coupling route	Phase composition, ZnO:CdS:$Cd(OH)_2$	Characterization of CdS NPs in ZnO NRs / CdS NPs composites			Conversion degree of HQ, %
			Particle size $< D >$*, nm	Crystal structure	E_g, eV	
1	*in-situ* CBD at pH = 12.5	17 : 52 : 31	7	random close-packed	2.3	85
2	*in-situ* CBD at pH = 13.7	81 : 19 : 0	5	hexagonal close packed	2.4	79
3	*ex-situ* from pre-synthesized colloid solution of CdS NPs	99 : 1 : 0	< 2	amorphous	2.7	83

*The average particle size <D> was determined from XRD data using Debye-Scherrer formular [44].

confinement effect in the CdS NPs. The mean size of the CdS NPs in composites was observed to range from 2–7 nm. All synthesized ZnO NRs / CdS NPs composites show photocatalytic activity in the photooxidation of HQ in aqueous solution.

The most uniform fiber like morphology is observed for ZnO NRs / CdS NPs composite synthesized using *ex-situ* coupling (sample 3), but the CdS quantity (about 1 at.%) on ZnO NRs

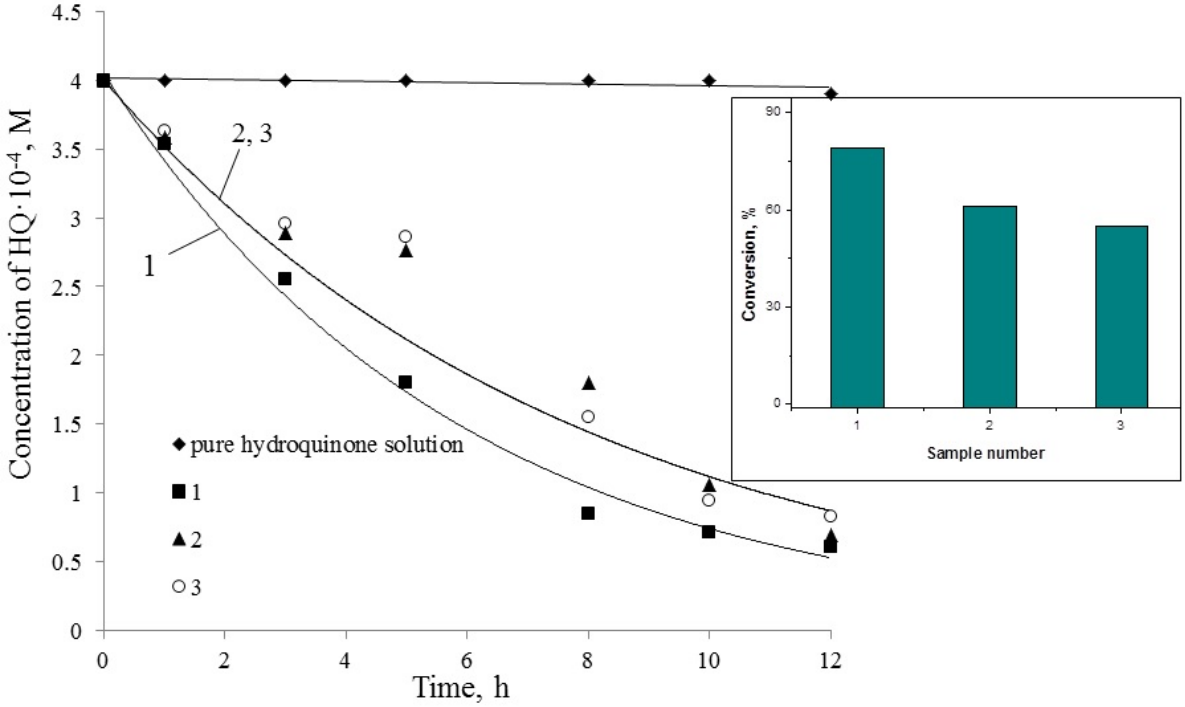

FIG. 4. The kinetics of catalytic oxidation of HQ aqueous solutions under visible light irradiation (440–460 nm) without and in presence of ZnO NRs / CdS NPs semiconductor composites (samples 1–3). The inset shows the conversion degree of hydroquinone to quinone via reaction $C_6H_4(OH)_2 + 0.5\ O_2 \Longleftrightarrow C_6H_4O_2 + H_2O$ after 8 hours of irradiation

is the smallest of three samples. The highest absorption intensity, rate and conversion degree in the photooxidation of HQ was observed for sample 1, obtained by CBD route and containing essential amount of $Cd(OH)_2$. The quantity of CdS NPs coupled with ZnO NRs in sample 1 is also the highest. On the one hand, $Cd(OH)_2$ forms one more crystal phase and violates the uniformity of composite microstructure. On the other, due to hydroxyl group it seems to play a role of bifunctional linker between ZnO and CdS and makes unnecessary additional surface treatment of ZnO NRs. This is important because despite of the porous structure of ZnO NRs, which helps in the coupling of CdS NPs, the number of CdS NPs reaches its maximum in the presence of $Cd(OH)_2$.

The chemical bath deposition technique of coupling ZnO NRs to CdS NPs presented in this work is advantageous, as it is a simple and efficient way to produce nanocrystalline semiconductor composites with controllable quantity and size of the nanoparticles, which could find use in large area surface coatings for advanced photocatalytic and solar cell materials.

Acknowledgements

This work is partially financially supported by RFBR (Project No. 12-03-00453-a).

References

[1] Hu L., Yan J., et al. An optimized ultraviolet -A light photodetector with wide range photoresponse based on ZnS/ZnO biaxial nanobelt. *Adv. Mater.*, **24** (17), P. 2305–2309 (2012).

[2] Panda S.K., Chakrabarti S., et al. Optical and microstructural characterization of CdS-ZnO nanocomposite thin films prepared by sol-gel technique. *J. Phys. D: Appl. Phys.*, **37** (4), P. 628–633 (2004).

[3] Fang X., Bando Y., et al. Inorganic semiconductor nanostructures and their field-emission applications. *J. Mater. Chem.*, **18** (5), P. 509–522 (2008).
[4] Hoffmann M. R., Martin S. T., Choi W., Bahnmann D. W. Environmental applications of semiconductor photocatalysis. *Chem. Rev.*, **95** (1), P. 69–96 (1995).
[5] Fang X., Wu L., Hu L. ZnS nanostructure arrays: a developing material star. *Adv. Mater.*, **23** (5), P. 585–598 (2011).
[6] Liu H., Hu L., et al. Cathodoluminescence modulation of ZnS nanostructures by morphology, doping and temperature. *Adv. Funct. Mater.*, **23** (29), P. 3701–3709 (2013).
[7] Jiang C.Y., Sun X.W., et al. Improved dye-sensitized solar cells with a ZnO-nanoflower photoanode. *Appl. Phys. Lett.*, **90** (26), P. 263501 (2007).
[8] Pan Z.W., Dai Z.R., Wang Z.L. Growth and structure evolution of novel tin oxide diskettes. *J. Am. Chem. Soc.*, **124** (29), P. 8673–8680 (2002).
[9] Pan Z.W., Dai Z.R., Wang Z.L. Nanobelts of semiconducting oxides. *Science*, **291** (5510), P. 1947–1949 (2001).
[10] Aroutiounian V. M., Arakelyan V. M., Shahnazaryan G. E. Metal oxide photoelectrodes for hydrogen generation using solar radiation-driven water splitting. *Sol. Energy*, **78** (5), P. 581–592 (2005).
[11] Jana T.K., Pal A., Chatterjee K. Self-assembled flower like CdS-ZnO nanocomposite and its photocatalytic activity. *J. Alloys and Compounds*, **583**, P. 510–515 (2014).
[12] Khanchandani S., Kundu S., Patra A., Ganguli A.K. Band gap tuning of ZnO/In_2S_3 core/shell nanorod arrays for enhanced visible-light-driven photocatalysis. *J. Phys. Chem. C*, **117** (11), P. 5558–5567 (2013).
[13] Balachandran S., Swaminathan M. Facile fabrication of heterostructured Bi_2O_3–ZnO photocatalyst and its enhanced photocatalytic activity. *J. Phys. Chem. C*, **116** (50), P. 26306–26312 (2012).
[14] Khanchandani S., Kundu S., Patra A., Ganguli A.K. Shell thickness dependent photocatalytic properties of ZnO/CdS core-shell nanorods. *J. Phys. Chem. C*, **116** (44), P. 23653–23662 (2012).
[15] Wang L., Wei H., et al. Synthesis, optical properties and photocatalytic activity of one-dimensional CdS@ZnS core-shell nanocomposites. *Nanoscale Res. Lett.*, **4** (6), P. 558–564 (2009).
[16] Barpuzary D., Khan Z., et al. Hierarchically grown urchinlike CdS@ZnO and CdS@Al_2O_3 heteroarrays for efficient visible light-driven photocatalytic hydrogen generation. *J. Phys. Chem. C*, **116** (1), P. 150–156 (2012).
[17] Fujii H., Ohtaki M., Eguchi K., Arai H. Preparation and photocatalytic activities of a semiconductor composite of CdS embedded in a TiO_2 gel as a stable oxide semiconducting matrix. *J. Mol. Catal. A: Chem.*, **129** (1), P. 61–68 (1998).
[18] Kamat P.V. Photochemistry on nonreactive and reactive (semiconductor) surfaces. *Chem. Rev.*, **93** (1), P. 267–300 (1993).
[19] Gopidas K.R., Bohorquez M., Kamat P.V. Photophysical and photochemical aspects of coupled semiconductors: charge-transfer processes in colloidal cadmium sulfide-titania and cadmium sulfide-silver(I) iodide systems. *J. Phys. Chem.*, **94** (16), P. 6435–6440 (1990).
[20] Evans J.E., Springer K.W., Zhang J.Z. Femtosecond studies of interparticle electron transfer in a coupled CdS-TiO2 colloidal system. *J. Chem. Phys.*, **101** (7), P. 6222–6225 (1994).
[21] Sudhagar P., Chandramohan S., et al. Fabrication and charge-transfer characteristics of CdS QDs sensitized vertically grown flower-like ZnO solar cells with CdSe cosensitizers. *Phys. Stat. Sol. A*, **208** (2), P. 474–479 (2011).
[22] Jun H.K., Careem M.A., Arof A.K. Quantum dot-sensitized solar cells — perspective and recent developments: A review of Cd chalcogenide quantum dots as sensitizers. *Renewable and Sustainable Energy Reviews*, **22**, P. 148–167 (2013).
[23] Qi X., She G., et al. Electrochemical synthesis of CdS/ZnO nanotube arrays with excellent photoelectrochemical properties. *Chem. Commun.*, **48** (2), P. 242–244 (2012).
[24] Kundu P., Deshpande P.A., Madras G., Ravishankar N. Nanoscale ZnO/CdS heterostructures with engineered interfaces for high photocatalytic activity under solar radiation. *J. Mater. Chem.*, **21** (12), P. 4209–4216 (2011).
[25] Tak Y., Hong S.J., Lee J.S., Yong K. Solution-based synthesis of a CdS nanoparticle/ZnO nanowire heterostructure array. *Cryst. Growth Des.*, **9** (6), P. 2627–2632 (2009).
[26] Tak Y., Kim H., Lee D., Yong K. Type-II CdS nanoparticle-ZnO nanowire heterostructure arrays fabricated by a solution process: enhanced photocatalytic activity. *Chem. Commun.*, **38**, P. 4585–4587 (2008).
[27] Hodes G. Comparison of dye- and semiconductor-sensitized porous nanocrystalline liquid junction solar cells. *J. Phys. Chem. C*, **112** (46), P. 17778–17787 (2008).

[28] Niitsoo O., Sarkar S.K., et al. Chemical bath deposited CdS/CdSe-sensitized porous TiO_2 solar cells. *J. Photochem. Photobiol. A*, **181** (2–3), P. 306–313 (2006).
[29] Nicolau Y.F., Dupuy M., Brunel M. ZnS, CdS and $Zn_{1-x}Cd_xS$ thin films deposited by the successive ionic layer adsorption and reaction process. *J. Electrochem. Soc.*, **137** (9), P. 2915–2924 (1990).
[30] Robel I., Subramanian V., Kuno M., Kamat P.V. Quantum dot solar cells. Harvesting light energy with CdSe nanocrystals molecularly linked to mesoscopic TiO_2 films. *J. Am. Chem. Soc.*, **128** (7), P. 2385–2393 (2006).
[31] Gyrdasova O.I., Krasil'nikov V.N., et al. Synthesis, microstructure, and photocatalytic characteristics of quasi-one-dimensional zinc oxide doped with d elements. *Doklady Chemistry*, **434** (1), P. 211–213 (2010).
[32] Melkozerova M.A., Krasil'nikov V.N., et al. Effect of doping with 3d elements (Co, Ni, Cu) on the intrinsic defect structure and photocatalytic properties of nanostructured ZnO with tubular morphology of aggregates. *Physics of the Solid State*, **55** (12), P. 2459–2465 (2013).
[33] Shalaeva E.V., Gyrdasova O.I., et al. Structural, optical, and photocatalytic properties of quasi-one-dimensional nanocrystalline ZnO, ZnOC:nC composites, and C-doped ZnO. In: Nanocomposites, Nanophotonics, Nanobiotechnology, and Applications. Springer Proceedings in Physics, **156**, (26), DOI 10.1007/978-3-319-06611-0_26 (2014) (in press).
[34] Kozhevnikova N.S., Vorokh A.S., Rempel A.A. Preparation of stable colloidal solution of cadmium sulfide CdS using ethylenediaminetetraacetic acid. *Russ. J. General Chem.*, **80** (3), P. 391–394 (2010).
[35] Rempel A.A., Kozhevnikova N.S., Rempel S.V. Structure of cadmium sulfide nanoparticle micelle in aqueous solutions. *Russ. Chem. Bulletin*, **62** (2), P. 398–402 (2013).
[36] Kitaev G.A., Morkrushin S.G., Uritskarya A.A. Chemical bath deposition conditions of CdS thin films on solid surface. *Russ. J. Phys. Chem.*, **39** (8), P. 2065–2066 (1965).
[37] Ortega-Borges R., Lincot D. Mechanism of chemical bath deposition od cadmium sulfide thin films in ammoni-thiourea system. *J. Electrochem. Soc.*, **140** (12), P. 3464–3473 (1993).
[38] Chapman A.J., Lane D.W., Rogers K.D., Özsan M.E. Microstructural changes of CdTe during the annealing process. *Thin Solid Films*, **403–404**, P. 522–525 (2002).
[39] Yan Y., Albin D., Al-Jassim M.M. Do grain boundaries assist S diffusion in polycrystalline CdS/CdTe heterojunctions? *Appl. Phys. Lett.*, **78** (2), P. 171–173 (2001).
[40] O'Brien P., Saeed T.J. Deposition and characterization of cadmium sulfide thin films by chemical bath deposition. *J. Cryst. Growth*, **158** (4) P. 497–504 (1996).
[41] Thavasi V., Renugopalakrishnan V., Jose R., Ramakrishna S. Controlled electron injection and transport at materials interfaces in dye sensitized solar cells. *Mater. Sci. Eng. R*, **63** (3), P. 81–99 (2008).
[42] Vorokh A.S., Rempel A.A. Direct-space visualization of the short and 'average' long-range orders in the noncrystalline structure of a single cadmium sulfide nanoparticle. *JETF Letters*, **91** (2), P. 100–104 (2010).
[43] Ukhanov Yu.I. *Optical Properties of Semiconductors*. Nauka, Moscow, 1977, 366 p. (in Russian).
[44] Vorokh A.S., Rempel A.A. Atomic structure of cadmium sulfide nanoparticles. *Phys. Solid State*, **49** (1), P. 148–153 (2007).